AN EXCITABLE ELECTRONIC CIRCUIT AS A SENSORY NEURON MODEL

BRUNO N. S. MEDEIROS*, VICTOR MINCES†, GABRIEL B. MINDLIN‡,
MAURO COPELLI* and JOSÉ R. RIOS LEITE*

*Departamento de Física, Universidade Federal de Pernambuco,
50670-901 Recife, PE, Brazil

†Department of Cognitive Neuroscience, University of California San Diego,
92093-0515 La Jolla, CA, USA

‡Departamento de Física, FCEN, Universidad de Buenos Aires,
Ciudad Universitaria, Pab. I, 1428 Buenos Aires, Argentina

An electronic circuit device, inspired on the FitzHugh–Nagumo model of neuronal excitability, was constructed and shown to operate with characteristics compatible with those of biological sensory neurons. The nonlinear dynamical model of the electronics quantitatively reproduces the experimental observations on the circuit, including the Hopf bifurcation at the onset of tonic spiking. Moreover, we have implemented an analog noise generator as a source to study the variability of the spike trains. When the circuit is in the excitable regime, coherence resonance is observed. At sufficiently low noise intensity the spike trains have Poisson statistics, as in many biological neurons. The transfer function of the stochastic spike trains has a dynamic range of 6 dB, close to experimental values for real olfactory receptor neurons.

Keywords: Electronic circuit; excitable element; coherence resonance; dynamic range.

1. Introduction

Ever since the pioneering work of Hodgkin and Huxley [1952], the biophysical mechanisms underlying the generation and propagation of action potentials (spikes) in neurons have been described with increasing detail, ranging from the discovery of new types of ion channels to the study of intracellular calcium dynamics [Hille, 2001]. No matter how interesting, these new findings have helped little in our understanding of collective neuronal phenomena, which remain a daunting task in face of the interplay among high-dimensionality, noise and nonlinearity (see e.g. [Chialvo, 2010] for a recent review). The challenge should nonetheless be faced: the solution of issues at the frontiers of current-day neuroscience, like e.g. grandmother cell [Barlow, 1972] versus population coding [Young & Yamane, 1992], or firing rate versus spike-time coding

[Rieke *et al.*, 1999] will likely be grounded on our success in this endeavor.

In fact, theoretical progress in this front has been achieved in recent years with very simple models. One such example is the proposed solution for the century-old problem of the origin of psychophysical response curves [Copelli *et al.*, 2002; Kinouchi & Copelli, 2006]. Steven's psychophysical law states that the psychological perception F of a physical stimulus (e.g. light, or odorant) of intensity h is a power law $F \propto h^s$, with experimental values of the Stevens exponent s fluctuating around $s \simeq 0.5$. Compared to a linear response, psychophysical nonlinear responses have at least one evolutionarily favorable property: they amplify weaker stimulus, i.e. they have a larger dynamic range. But how do the Stevens exponents arise in the nervous system?

At first, this question seems puzzling because single neurons typically have small dynamic ranges [Rospars *et al.*, 2000]. A theoretical solution recently proposed involves a collective phenomenon: excitable waves are generated by the incoming stimuli and propagate "laterally" among excitable neurons, thereby amplifying the system response (in comparison to what would be observed in the absence of the coupling). Interestingly, this amplification mechanism is self-limited: under intense stimulation, for instance, a large number of excitable waves can be created, but owing to refractoriness they annihilate upon collision. The enhancement of dynamic range in this model is therefore governed by the low-stimulus amplification [Copelli *et al.*, 2002; Kinouchi & Copelli, 2006]. Robustness of these results has been tested at different modeling levels [Copelli *et al.*, 2005; Ribeiro & Copelli, 2008; Assis & Copelli, 2008; Publio *et al.*, 2009], showing that the degree of biophysical realism in the model of each neuron is less relevant to the global dynamics than the topology of the network [Copelli & Kinouchi, 2005; Copelli & Campos, 2007; Ribeiro & Copelli, 2008; Assis & Copelli, 2008; Gollo *et al.*, 2009]. This phenomenon has also been studied analytically [Furtado & Copelli, 2006; Larremore *et al.*, 2011] and was recently confirmed experimentally in cortical slices [Shew *et al.*, 2009].

The appeal of a sensory system with large dynamic range based on a network of simple excitable units, each with small dynamic range, goes beyond basic research in neuroscience. The idea could be reversed, leading to biologically inspired artificial sensors, which have been used in a variety of scenarios (see e.g. [de Souza *et al.*, 1999]).

There are several electronic circuits reported in the literature which have been designed to present a neuron-like dynamical response. The rationale behind those efforts was to dynamically interact with biological neurons rather than stimulating them using response independent current commands. In this way, electronic circuits which analogically integrated the Hindmarsh and Rose equations [Szucs *et al.*, 2000] were coupled to the neurons of a preparation of lobster pyloric CPG neurons. This allowed to show that regularity could emerge as a collective dynamical property of units which individually presented complex dynamics. In another set of experiments, electronic neurons interacting with a biological preparation were used to unveil which dynamical properties of a neural

network depend on the bifurcation leading to excitation for the units, rather than on the details of the neural dynamics. To carry out this program, a standard form for class I excitable dynamics was analogically integrated with a circuit, which was used to replace a neuron in a midbody ganglion of the leech Hirudo medicinalis [Aliaga *et al.*, 2003]. The responses under the stimulation of both the natural preparation and the one with a replaced neuron were found to be similar. Beyond the possibility of interacting with neurons through a dynamically sensible way, these efforts provide empirical support to the program of studying neural processes through simple and relatively low-dimensional dynamical systems. Depending on the question under study, it might be desirable to be able to establish a closer link between the device and a neuron. In this spirit, a device implementing a conductance model was recently proposed [Sitt & Aliaga, 2007].

These circuits, however, have two limitations for our purposes. First, they are still too complex to be replicated in large scale. Second, they do not have a controllable noise source to produce stochastic spike trains, a feature that is common to both models [Copelli *et al.*, 2002] and real neurons [Dayan & Abott, 2001; Mainen & Sejnowski, 1995; Petracchi *et al.*, 1995]. The present work is a first step in this direction. We propose an excitable electronic circuit which can serve as a building block of an electronic sensor. The advantages of its extreme simplicity are two-fold: it allows for scalability and, at the same time, simple mathematical modeling.

The paper is organized as follows. In Sec. 2, we describe the electronic circuit and the equations that model its dynamics. In Sec. 3, we introduce noise from a simple analog noise generator at the input of the excitable circuit and study the statistical properties of the resulting spike trains and show that it can exhibit Poisson statistics as well as coherence resonance, as expected. In Sec. 4, we evaluate the dynamic range of the excitable circuit and show that it is comparable to that of single sensor neurons.

2. Dynamic Model

The circuit we propose is shown in Fig. 1. It is composed of five resistors, one capacitor and one operational amplifier. The voltage V_{in} corresponds to an external stimulus, which can be e.g. a constant or the sum of DC and noise voltages. In our electronic
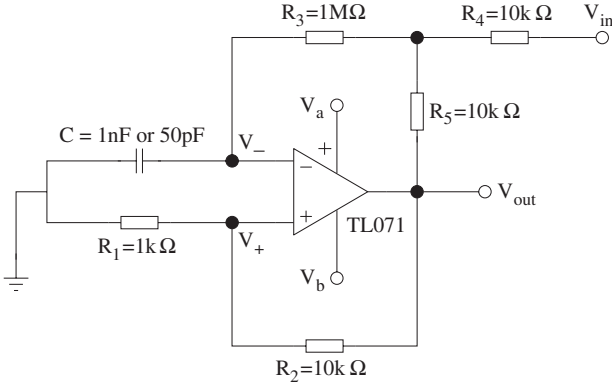
Fig. 1. Excitable electronic circuit. V_a and $V_b = -V_a$ are the operational amplifier supply voltages. V_{in} is an input voltage, corresponding to an external stimulus. We describe the circuit as a two-dimensional dynamical system on the variables V_- and V_{out} [see Eqs. (2)].

neuron, the operational amplifier behaves as a simple comparator circuit, for which we use the following nonlinear model:

$$\frac{dV_{out}}{dt} = S\,\mathrm{sign}[V_b - V_{out}$$
$$+ (V_a - V_b)\Theta(V_+ - V_-)], \qquad (1)$$

where Θ is the Heaviside function and S is the op-amp slew rate (whose datasheet value for the simple TL071 in the circuit is $S = 16\,\mathrm{V/s}$). As usual, symmetric supply voltages $V_b = -V_a$ were used.

Assuming $R_3 \gg R_4, R_5$ and applying Kirchhoff's laws, we arrive at a two-dimensional dynamic model on the variables V_{out} and V_-:

$$\frac{dV_{out}}{dt} = \frac{V_c}{\varepsilon}\mathrm{sign}[V_b - V_{out}$$
$$+ (V_a - V_b)\Theta(\alpha V_{out} - V_-)], \qquad (2a)$$

$$\frac{dV_-}{dt} = \frac{1}{R_3 C}[\beta V_{out} + \gamma V_{in} - V_-]. \qquad (2b)$$

where $\alpha \equiv R_1/(R_1 + R_2)$, $\beta \equiv R_4/(R_4 + R_5)$ and $\gamma \equiv R_5/(R_4 + R_5)$. $V_c = 10\,\mathrm{V}$ is a characteristic voltage of the same order of magnitude of the supply voltages, and we have defined $\varepsilon \equiv V_c/S$ as a characteristic (short) time scale. To avoid the possibility that the system (2) has more than one fixed point, we require $\beta > \alpha$. In terms of the variables

$$v \equiv \frac{V_{out}}{V_c}, \qquad (3a)$$

$$w \equiv \frac{V_-}{V_c}, \qquad (3b)$$

the equations can be rewritten in dimensionless form

$$\dot{v} = \mathrm{sign}\left(b - v + \frac{(a-b)}{1 + e^{-(\alpha v - w)/x_0}}\right), \qquad (4a)$$

$$\dot{w} = \phi[\beta v + \gamma j - w], \qquad (4b)$$

where we defined the dimensionless groups:

$$\tau \equiv \frac{t}{\varepsilon}; \quad a = \frac{V_a}{V_c}; \quad b = \frac{V_b}{V_c};$$
$$\phi = \frac{\varepsilon}{R_3 C}; \quad j = \frac{V_{in}}{V_c}, \qquad (5)$$

and replaced Θ by the continuous function

$$\tilde{\Theta}(x; x_0) = \frac{1}{1 + e^{-x/x_0}} \qquad (6)$$

for the purpose of numerical integration and derivation (see below). Note that $\tilde{\Theta} \to \Theta$ as $x_0 \to 0$. The constant $\phi \ll 1$ sets the ratio between the fast and slow time scales as in the FitzHugh–Nagumo model, so that $R_3 C$ ultimately controls the overall time scale of the problem.

As shown in Fig. 2(a) (black lines), the nullclines $\dot{v} = 0$ and $\dot{w} = 0$ of Eqs. (4) resemble those of the FitzHugh–Nagumo model for neuronal excitability, with one fast (v or V_{out}) and one slow (w or V_-) variable. In the limit $x_0 \to 0$, the cubic-like $\dot{v} = 0$ nullcline becomes piecewise linear. When the fixed point sits at its outer branches, it is stable. It loses stability in a Hopf bifurcation as the w nullcline crosses the v nullcline at its central branch, so trajectories are attracted to a limit cycle (red line) with nonzero frequency f (i.e. f changes discontinuously at the bifurcation). Below the Hopf bifurcation, the circuit is said to be type-II excitable [Rinzel & Ermentrout, 1998].

There is good quantitative agreement between experimental data from the circuit and the numerical integration, as can be seen in Figs. 2(b)–2(e). Note that through an analog subtraction $V_m \equiv 1.5V_- - 0.67V_{out}$ [see also Fig. 3(b)] the circuit exhibits the spikes typical of neuronal membrane potentials [Fig. 2(e)]. We emphasize that in Fig. 2 experimental and numerical data agree without any fitting parameter, as long as x_0 is sufficiently small ($\lesssim 10^{-4}$).
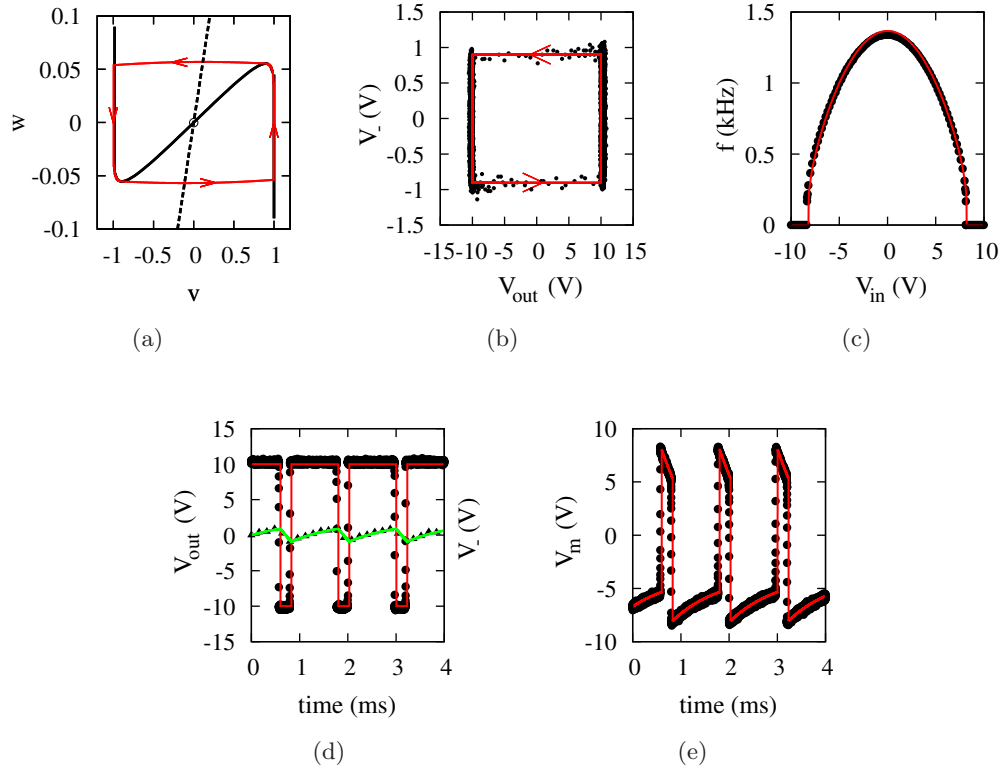
(a)

(b)

(c)

(d)

(e)

Fig. 2. (a) Nullclines of system (4) for $a = 1$, $b = 1$, $\alpha = 0.0909$, $\beta = 0.5$, $\gamma = 0.5$, $j = 0$, $\phi = 0.01$ and $x_0 = 9 \times 10^{-3}$: solid black line for the $\dot{v} = 0$ nullcline and dashed black line for the $\dot{w} = 0$ nullcline. The fixed point is unstable and the trajectories are attracted to a limit cycle (red solid line). (b) Experimental limit cycle (black dots) and numerical integration of the model (red solid line) for $x_0 = 1 \times 10^{-5}$, $V_a = 10\,\mathrm{V}$, $V_b = -10\,\mathrm{V}$, $V_{\mathrm{in}} = -6\,\mathrm{V}$ and $\phi = 5 \times 10^{-4}$ (other parameters are the same as in (a)). (c) Experimental frequency response f to the external DC stimulus V_{in} (black dots) and the same for the numerical integration of the model (red line). (d) Comparison between experimental time series of V_{out} and V_- (black circles and triangles, respectively) with numerical integration of the model (red and green lines, respectively). (e) Experimental (black dots) and numerical (red line) spike trains obtained from the analog subtraction V_m of the dynamical variables (see text for details).

3. Noise Addition and Coherence Resonance

So far we have discussed the response of the excitable circuit under DC stimulation. Biological neurons, however, can show highly variable responses, even when subjected to a presumably constant stimulus. Examples range from highly variable responses of olfactory receptor neurons (ORNs) to the presentation of identical puffs of odorants [Rospars *et al.*, 2000], to cortical cells stimulated with a constant current via an intracellular electrode [Mainen & Sejnowski, 1995]. In an attempt to endow our excitable circuits with the variability in the spike trains observed in biological neurons, we propose the simple analog noise generator shown in Fig. 3(a). Once more, its simplicity allows one to attach independent noise generators to each excitable circuit when connecting them in a network.

The circuit in Fig. 3(a) provides a two-stage amplification control via two operational amplifiers to the thermal noise produced by the KN2222 transistors. Its output voltage V_{noise} is approximately a Gaussian white noise voltage with a cutoff frequency around 1 kHz.

To obtain variable spike trains, the stimulus V_{in} consists in the analog addition of V_{DC} and V_{noise} [see blocks 1 and 2 in Fig. 3(b)]. In the model, this corresponds to replacing Eq. (4b) with

$$\dot{w} = \phi[\beta v + \gamma j + D\xi(t) - w], \qquad (7)$$

where D grows linearly with the gain in the noise amplification A (which in turn is controlled by the variable resistors shown in Fig. 3).

Setting V_{DC} below the Hopf bifurcation, the circuit sits at a stable fixed point at the right branch of the $\dot{v} = 0$ nullcline, from which it eventually departs owing to noise [Fig. 4(a)]. This generates
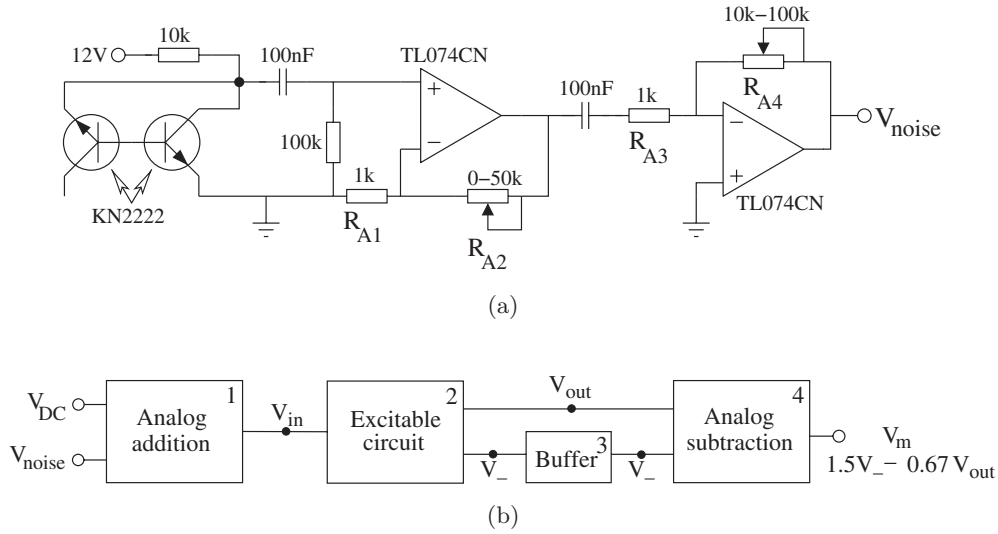
(a)

(b)

Fig. 3. (a) An analog noise generator based on the amplification of transistors thermal noise. Noise amplification is given by $A = [(R_{A1} + R_{A2})/R_{A1}](R_{A4}/R_{A3})$. (b) Block diagram of the circuit used to verify the excitability of the circuit presented in Fig. 1. Analog addition and subtraction (see text for details) are performed with standard TL074 op-amp operations [Senturia & Wedlock, 1981].

spike trains with variable interspike intervals t_p, as shown in Figs. 4(b) and 4(c).

We now show that the interplay between noise and excitability behaves as expected in our simple circuits. Pikovsky and Kurths [1997] have shown the coherence of the spike train of the FitzHugh–Nagumo model peaks at an intermediate noise value, in a phenomenon which has been called
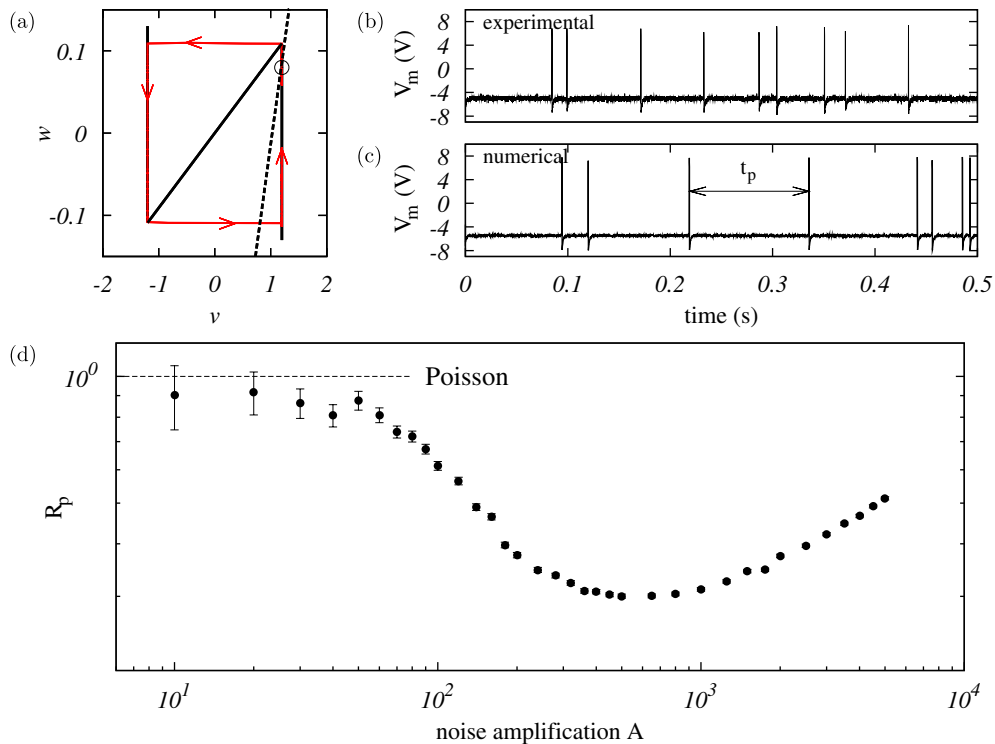

Fig. 4. (a) Numerical phase plane trajectory (red line) due to noise excitation. Without noise, the system would stay in a resting state at the fixed point (white circle). (b) Experimental and (c) numerical spike train series are shown when the system is in the excitable state (stable fixed point as shown in (a)). (d) Experimental coherence resonance curve for $C = 50\,\text{pF}$, $V_a = 12\,\text{V} = -V_b$ and $V_{DC} = -7.826\,\text{V}$ (see Fig. 1). Each point corresponds to an average over 10 s time series.

"coherence resonance". In other words, the normalized standard deviation

$$R_p \equiv \frac{\sqrt{\langle t_p^2 \rangle - \langle t_p \rangle^2}}{\langle t_p \rangle} \tag{8}$$

should have a minimum as a function of the noise intensity. This is precisely what we observe in our circuit when V_{DC} ($= -7.826\,\mathrm{V}$) is close to the Hopf bifurcation ($V_{\mathrm{Hopf}} = -7.82\,\mathrm{V}$), as displayed in Fig. 4(d). Note that R_p close to zero means that the time series is approximately periodic.

For small noise amplitudes [$V_{\mathrm{noise}} \sim 50\,\mathrm{mV}$, or $A \sim \mathcal{O}(1)$ in Fig. 4(d)], spikes are sparse and R_p approaches unity. This suggests a Poisson process in which the interspike interval distribution approaches an exponential

$$P(t_p) = r e^{-r t_p}, \tag{9}$$

where r is time rate constant. This Poisson limit is interesting because it is observed in different neuronal preparations [Dayan & Abott, 2001; Petracchi *et al.*, 1995], so we performed a detailed statistical analysis of the small V_{noise} regime.

In Fig. 5(a) the statistics of a 100 s experimental time series was compared to the accumulated distribution

$$D(t) \equiv \int_t^\infty r e^{-r t_p} dt_p = e^{-rt}, \tag{10}$$

showing good agreement for a fitted rate $r \simeq 10.0(3)\,\mathrm{s}^{-1}$. To check for consistency, we divided the time series in small time windows of size T and sampled the number n of spikes per window. In a Poisson process one has the linear relationships $\langle n \rangle = rT$, $\sigma_n^2 \equiv \langle n^2 \rangle - \langle n \rangle^2 = rT$ which are confirmed in Figs. 5(b) and 5(c). The unit slope in the
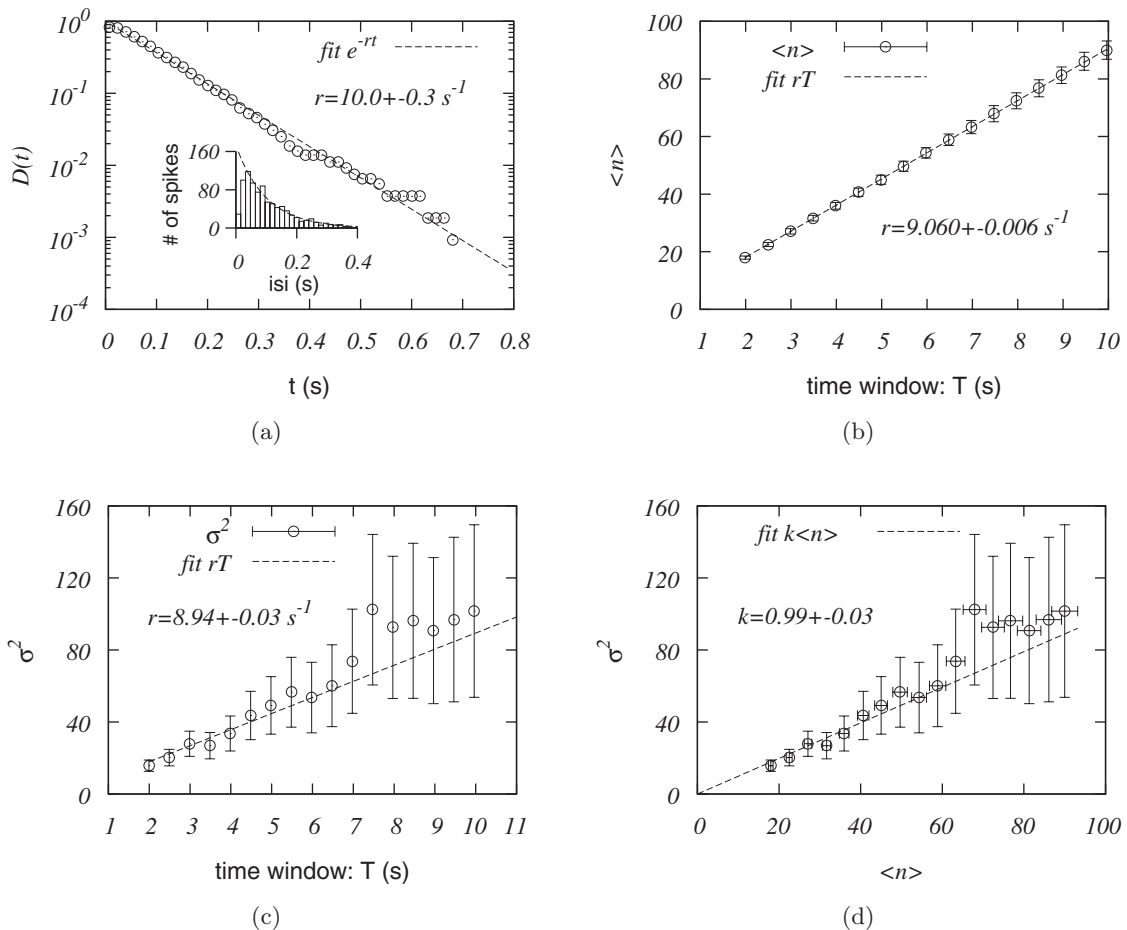

Fig. 5. Spike train statistics of a 100 s duration series from the circuit of Fig. 3(b). (a) Interspike interval (isi) accumulated distribution in log-linear scale. Inset: corresponding histogram of isi. The dashed line corresponds to an exponential fit of a Poisson distribution with mean firing rate $r = 10.0(3)\,\mathrm{s}^{-1}$. The deviation from the Poisson distribution for small isi is due to the refractoriness of the excitable circuit. In the following graphs we have divided the series in time windows of duration T. (b) The mean number of spikes $\langle n \rangle$ and (c) the variance σ^2 are shown as functions of T. In (d) we have σ^2 as a function of $\langle n \rangle$. The dashed lines are fits of $\sigma^2 = \langle n \rangle = rT$ according to the Poisson distribution.

σ_n^2 versus $\langle n \rangle$ plot is also verified [see Fig. 5(d)]. These results show that our circuit can be used to mimic not only deterministic dynamics, but also simple statistical properties which appear in biological neurons.

4. Dynamic Range

In this section, we study the response of our excitable system to varying input voltage V_{DC}, considering the noise amplitude V_{noise} constant. Although in real neurons the background noise may have a dependence on the stimulus, it is a fair approximation to treat the noise amplitude as constant and focus on the dependence on input signal as a control parameter of the dynamics. In what follows, the response of the circuit is defined as

the mean firing rate F measured over a fixed time interval T_m. This so-called "rate coding" is also a longstanding approximation [Adrian, 1926], which seems to fit data in several cases [Koch, 1999; Arbib, 2002].

For fixed T_m and noise amplification A, the response F of our circuit is an increasing function of the stimulus V_{DC} because larger values of V_{DC} amounts to increased excitability, lowering the "effective threshold" to noise-induced spike generation (there is no real threshold in type-II excitable neurons [Izhikevich, 2007]). Conversely, for fixed V_{DC}, the response F also increases with increasing noise intensity A. These results are shown in Fig. 6(a), where we plot (for different noise intensities) the responses $F(V_{DC})$ of our excitable circuit with a 1 nF capacitor. This choice sets the time
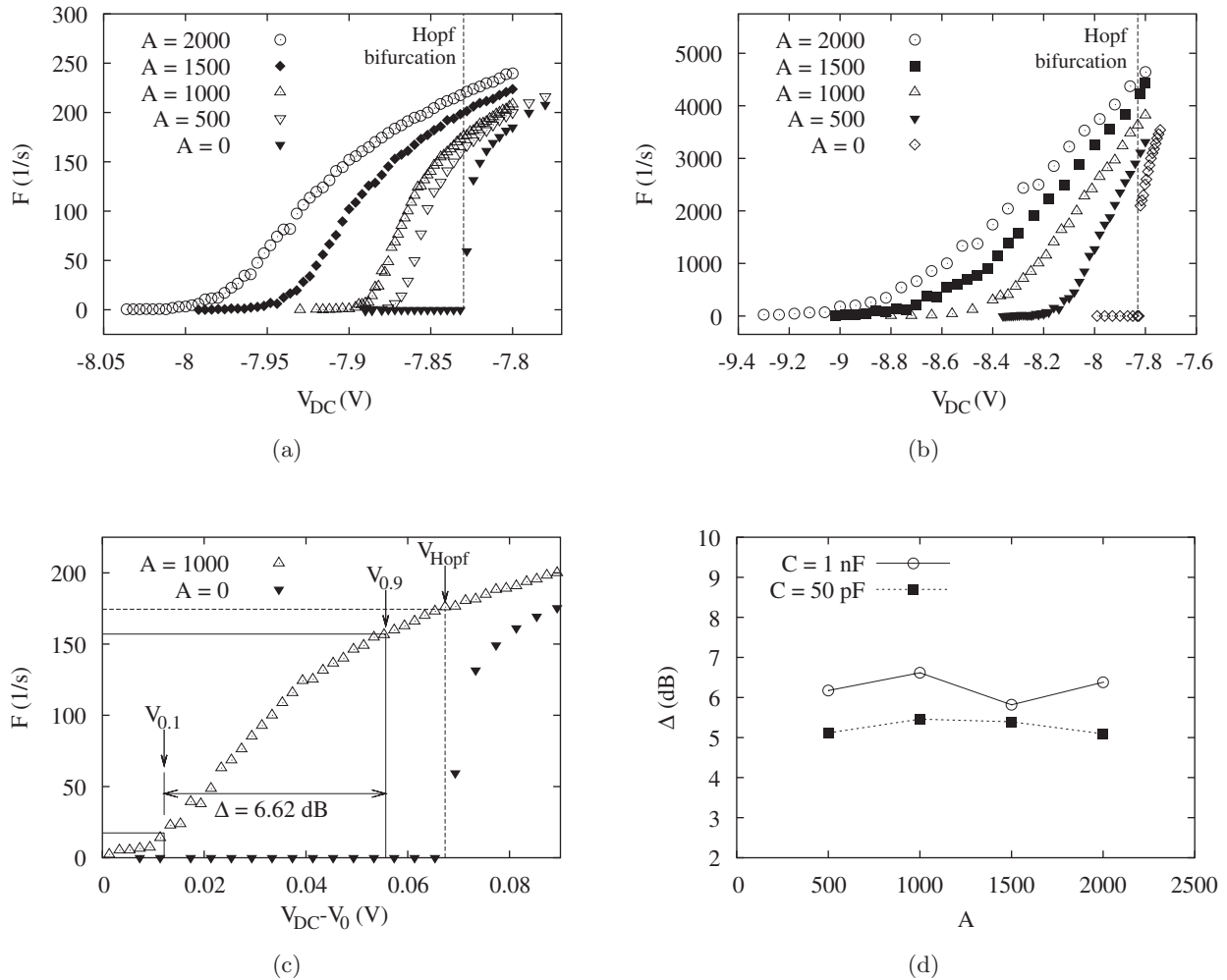

Fig. 6. Experimental response curves $F(V_{DC})$ measured at different values of the noise amplification A. Supply voltages $V_a = 12\,V = -V_b$. (a) $C = 1\,nF$ ($\phi = 5 \times 10^{-4}$ and $T_m = 10\,s$). (b) $C = 50\,pF$ ($\phi = 0.01$ and $T_m = 0.2\,s$). (c) Response curve for $C = 1\,nF$ ($A = 1000$), and relevant parameter for calculating the dynamic range. (d) Dynamic range as function of noise amplification for $C = 50\,pF$ (black squares) and $C = 1\,nF$ (white circles).

scale of the neuron in the millisecond range (i.e. that of biological neurons). Note that in the absence of noise ($A = 0$) the response is null up to the Hopf bifurcation [so the lowest curve in Fig. 6(a) is similar to Fig. 2(c)].

Results in Fig. 6(b) correspond to a circuit with a 50 pF capacitor. This single change renders a much faster circuit, now operating in the microsecond range, but with its dynamical features otherwise preserved. This has potential applications, because a faster circuit requires shorter measurement intervals T_m ($= 0.2$ s in our example) for a reliable estimation of the firing rate.

Given a response curve, we can calculate its dynamic range, which roughly speaking corresponds to the range of stimulus intensity that the firing rate can "appropriately code". Measured in decibels, this is arbitrarily defined as [Rospars *et al.*, 2000; Copelli & Kinouchi, 2005]

$$\Delta \equiv 10 \log_{10} \left(\frac{V_{0.9}^*}{V_{0.1}^*} \right), \tag{11}$$

where $V_x^* \equiv V_x - V_0$ are measured relative to the voltage V_0 at which the response becomes nonzero and

$$F(V_x) = x F_{\max} \quad (0 \le x \le 1), \tag{12}$$

where $F_{\max}$ is the firing rate at the Hopf bifurcation. In other words [see Fig. 6(c)], Δ measures the range of stimulus V_{DC} which are neither too small ($V_{\mathrm{DC}} < V_{0.1}$) to go undetected nor too close ($V_{\mathrm{DC}} > V_{0.9}$) to the autonomous oscillations that emerge at V_{Hopf}.

As shown in Fig. 6(d), the dynamic range is a rather robust feature of our excitable circuit: it changes little as the noise intensity is varied, regardless of the time scale at which it operates. In both cases, $\Delta \simeq 6$ dB, which is closer to the values obtained experimentally ($\Delta \simeq 10$ dB for olfactory sensory neurons [Rospars *et al.*, 2000], $\Delta \simeq 14$ dB for retinal ganglion cells [Deans *et al.*, 2002; Furtado & Copelli, 2006]) than results obtained theoretically for discrete models of excitable elements ($\Delta \simeq 14$ dB in [Furtado & Copelli, 2006] and $\Delta \simeq 19$ dB in [Assis & Copelli, 2008]).

5. Concluding Remarks

In summary, we have presented an excitable electronic circuit whose simplicity allows for scalability and accurate mathematical modeling. Its dynamical equations lead to time series which quantitatively reproduce experimental results without fitting parameters.

In addition, we have shown that the introduction of noise from a simple analog noise generator at the input of the circuit produces variable spike trains. The statistics of the interspike intervals is shown to exhibit coherence resonance. Furthermore, by analyzing long time series under low noise intensity, the spike trains were shown to behave as a Poisson process, like some biological neurons.

In the excitable regime, with fixed noise amplitude, the firing rate response of the system to a V_{DC} input — the stimulus — was shown to have a dynamic range of about 6 dB, which is also comparable to some biological sensory neurons. Together with its scalability, these properties render the system a potential building block for artificial sensors based on collective properties of excitable media.

Acknowledgments

References

Adrian, E. D. [1926] "The impulses produced by sensory nerve endings: Part I," *J. Physiol.* (*London*) **61**, 49–72.

Aliaga, J., Busca, N., Minces, V., Mindlin, G. B., Pando, B., Salles, A. & Sczcupak, L. [2003] "Electronic neuron within a ganglion of a leech (Hirudo medicinalis)," *Phys. Rev. E* **67**, 061915.

Arbib, M. A. [2002] *The Handbook of Brain Theory and Neural Networks* (MIT Press).

Assis, V. R. V. & Copelli, M. [2008] "Dynamic range of hypercubic stochastic excitable media," *Phys. Rev. E* **77**, 011923.

Barlow, H. B. [1972] "Single units and sensation: A neuron doctrine for perceptual psychology," *Perception* **1**, 371–394.

Chialvo, D. R. [2010] "Emergent complex neural dynamics," *Nature Phys.* **6**, 744–750.

Copelli, M., Roque, A. C., Oliveira, R. F. & Kinouchi, O. [2002] "Physics of psychophysics: Stevens and Weber–Fechner laws are transfer functions of excitable media," *Phys. Rev. E* **65**, 060901.

Copelli, M. & Kinouchi, O. [2005] "Intensity coding in two-dimensional excitable neural networks," *Physica A* **349**, 431–442.

Copelli, M., Oliveira, R. F., Roque, A. C. & Kinouchi, O. [2005] "Signal compression in the sensory periphery," *Neurocomputing* **65–66**, 691–696.

Copelli, M. & Campos, P. R. A. [2007] "Excitable scale-free networks," *Eur. Phys. J. B* **56**, 273–278.

Dayan, P. & Abott, L. F. [2001] *Theoretical Neuroscience*: *Computational and Mathematical Modeling of Neural Systems* (MIT Press).

Deans, M. R., Volgyi, B., Goodenough, D. A., Bloomfield, S. A. & Paul, D. L. [2002] "Connexin36 is essential for transmission of rod-mediated visual signals in the mammalian retina," *Neuron* **36**, 703–712.

de Souza, J. E. G., Neto, B. B., dos Santos, F. L., de Melo, C. P., Santos, M. S. & Ludermir, T. B. [1999] "Polypyrrole based aroma sensor," *Synth. Met.* **102**, 1296–1299.

Furtado, L. S. & Copelli, M. [2006] "Response of electrically coupled spiking neurons: A cellular automaton approach," *Phys. Rev. E* **73**, 011907.

Gollo, L. L., Kinouchi, O. & Copelli, M. [2009] "Active dendrites enhance neuronal dynamic range," *PLoS Comput. Biol.* **5**, e1000402.

Hille, B. [2001] *Ion Channels of Excitable Membranes*, 3rd edition (Sinauer Associates (Sunderland)).

Hodgkin, A. L. & Huxley, A. F. [1952] "A quantitative description of membrane current and its application to conduction and excitation in nerve," *J. Physiol.* **117**, 500–544.

Izhikevich, E. M. [2007] *Dynamical Systems in Neuroscience*: *The Geometry of Excitability and Bursting* (MIT Press, London).

Kinouchi, O. & Copelli, M. [2006] "Optimal dynamical range of excitable networks at criticality," *Nature Phys.* **2**, 348–351.

Koch, C. [1999] *Biophysics of Computation* (Oxford University Press, NY).

Larremore, D. B., Shew, W. L. & Restrepo, J. G. [2011] "Predicting criticality and dynamic range in complex networks: Effects of topology," *Phys. Rev. Lett.* **106**, 058101.

Mainen, Z. & Sejnowski, T. [1995] "Reliability of spike timing in neocortical neurons," *Science* **268**, 1503–1506.

Petracchi, D., Barbi, M., Chillemi, S., Pantazelou, E., Pierson, D., Dames, C., Wilkens, L. & Moss, F. [1995] "A test for a biological signal encoded by noise," *Int. J. Bifurcation and Chaos* **5**, 89–100.

Pikovsky, A. S. & Kurths, J. [1997] "Coherence resonance in a noise-driven excitable system," *Phys. Rev. Lett.* **78**, 775–778.

Publio, R., Oliveira, R. F. & Roque, A. C. [2009] "A computational study on the role of gap junctions and rod I_h conductance in the enhancement of the dynamic range of the retina," *PLoS ONE* **4**, e6970.

Ribeiro, T. L. & Copelli, M. [2008] "Deterministic excitable media under Poisson drive: Power law responses, spiral waves and dynamic range," *Phys. Rev. E* **77**, 051911.

Rieke, F., Warland, D., de Ruyter van Steveninck, R. & Bialek, W. [1999] *Spikes*: *Exploring the Neural Code* (MIT Press, Cambridge, MA).

Rinzel, J. & Ermentrout, B. [1998] "Analysis of neural excitability and oscillations," *Methods in Neuronal Modeling*: *From Ions to Networks*, eds. Koch, C. & Segev, I., 2nd edition (MIT Press), pp. 251–292.

Rospars, J.-P., Lánský, P., Duchamp-Viret, P. & Duchamp, A. [2000] "Spiking frequency versus odorant concentration in olfactory receptor neurons," *BioSyst.* **58**, 133–141.

Senturia, S. D. & Wedlock, B. D. [1981] *Electronic Circuits and Applications* (John Wiley).

Shew, W., Yang, H., Petermann, T., Roy, R. & Plenz, D. [2009] "Neuronal avalanches imply maximum dynamic range in cortical networks at criticality," *J. Neurosci.* **29**, 15595–15600.

Sitt, J. D. & Aliaga, J. [2007] "Versatile biologically inspired electronic neuron," *Phys. Rev. E* **76**, 051919.

Szucs, A., Varona, P., Volkovskii, A. R., Abarbanel, H. D. I., Rabinovich, M. & Selverston, A. I. [2000] "Interacting biological and electronic neurons generate realistic oscillatory rhythms," *Neuroreport* **11**, 563–569.

Young, M. & Yamane, S. [1992] "Sparse population coding of faces in the inferotemporal cortex," *Science* **256**, 1327–1331.